


Tight nonclassicality criteria for unbalanced Hanbury Brown–Twiss measurement scheme with click detectors

Jaromír Fiurášek *Department of Optics, Faculty of Science, Palacký University, 17. listopadu 12, 77900 Olomouc, Czech Republic* (Received 1 November 2023; revised 14 February 2024; accepted 27 February 2024; published 18 March 2024)

We derive tight nonclassicality criteria for an unbalanced Hanbury Brown–Twiss measurement scheme, where an input optical beam is split into two outputs on an unbalanced beam splitter. The outputs are measured with binary click detectors, such as avalanche photodiodes, that can distinguish the presence and absence of photons. Our nonclassicality criteria have the form of tight lower and upper bounds on probability p_{AB} of simultaneous no-clicks of both detectors for given probabilities p_A and p_B of no-clicks of the single detectors. These criteria are applicable to realistic detectors with limited detection efficiency. We show that the obtained criteria can detect nonclassicality of single-mode squeezed vacuum states.

DOI: [10.1103/PhysRevA.109.033713](https://doi.org/10.1103/PhysRevA.109.033713)

I. INTRODUCTION

Nonclassical states of light have attracted significant attention since the early days of quantum optics and they represent important resources in optical quantum technologies and quantum metrology. Nonclassical states of light are defined as states that cannot be expressed as mixtures of coherent states, i.e., the states for which the Glauber-Sudarshan P representation does not satisfy the properties of ordinary probability distribution. Characterization of nonclassical states of light and certification of their nonclassicality has a very long history yet it is still an important and active research topic today. The nonclassical states include important classes of states such as quadrature squeezed states or states with sub-Poissonian photon number distribution. Over the years a large number of nonclassicality criteria have been developed and experimentally tested based on photon statistics and photon counting measurements [1–12], moments of operators [13–18], phase-space quasidistributions and characteristic functions [19–25], or quantum coherence [26]. Various measures of nonclassicality have been proposed [27–30] and a resource theory of nonclassicality has been formulated [31]. Moreover, the concept of nonclassical states was extended to nonclassical measurements [32] that are defined as measurements the positive operator-valued measure (POVM) elements of which are not described in phase space by a positive well-behaved Glauber-Sudarshan P representation.

One of the conceptually simplest yet very important approaches is based on the Hanbury Brown–Twiss (HBT) measurement scheme [33], where the signal is split at a balanced beam splitter and the outputs are measured with single-photon detectors [1–3, 18] (see Fig. 1). For the input single-photon state one does not observe any coincidence clicks of the two detectors; only one of the detectors can click. This antibunching is a signature of nonclassicality and the measurement can be linked to detection of the normalized second-order correlation function $g^{(2)}(\tau)$, with the nonclassicality criterion $g^{(2)}(0) < 1$. One can even establish a lower

bound on the single-photon fraction in the state based on the value of $g^{(2)}(0)$ [18]. Going beyond nonclassicality, the HBT setup can be also used to certify quantum non-Gaussianity of the probed optical states [34]. In experiments with weak quantum light, detectors that can only distinguish the presence and absence of photons are commonly employed. The symmetric Hanbury Brown–Twiss setup then yields two independent probabilities that characterize the state: the probability that one of the detectors clicks (irrespective of the response of the other detector) and the probability that both detectors click simultaneously.

Interestingly, the information extractable from this measurement setup can be increased by using an unbalanced beam splitter, which breaks the symmetry [35]. This provides one additional parameter, because the probabilities of clicks of detectors D_A and D_B in Fig. 1 will no longer be the same. We thus get three independent parameters that characterize the observed state. In the present paper, we derive tight nonclassicality criteria based on full information extracted from an unbalanced Hanbury Brown–Twiss setup with binary click detectors. Formulation of the criteria is based on identification of the boundary of a convex set of probabilities of measurement outcomes that can be observed for classical states. In mathematical terms, this amounts to construction of a convex hull of a curve in a three-dimensional space [36–38].

Previously, nonclassicality criteria based on pairs of probabilities recorded with the Hanbury Brown–Twiss setup with click detectors were derived [6]. Also, nonclassicality criteria based on probability triples were obtained, by considering the probabilities of vacuum, single-photon, and two-photon states [11]. Finally, other nonclassicality criteria in multiparameter spaces were proposed very recently by going beyond the photon-number statistics and considering coherence-based criteria [26].

The rest of the paper is organized as follows. In Sec. II we review some basic facts and properties of nonclassicality detection with the HBT setup and binary click detectors. In Sec. III we provide general formulation of the nonclassicality

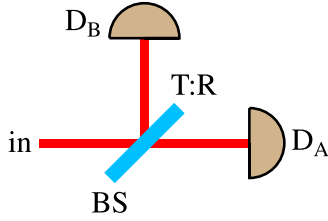


FIG. 1. Hanbury Brown–Twiss measurement scheme with click detectors. The input signal is split on a beam splitter BS into two output modes that are measured with binary on-off detectors D_A and D_B (such as avalanche photodiodes) that can distinguish the presence and absence of photons. Classical signals from detectors are processed to determine probabilities of clicks and no-clicks of various combinations of detectors. T and R denote the beam splitter intensity transmittance and reflectance, respectively. The auxiliary input port of BS is in a vacuum state.

criteria and relate them to the construction of convex hulls of specific three-dimensional curves. In Sec. IV we discuss the nonclassicality criteria for a specific setting with beam splitter transmittance $T = 1/3$ as in this case the calculations become particularly simple. We then generalize our analysis to arbitrary T in Sec. V. In Sec. VI we apply our criteria to certification of nonclassicality of the single-mode squeezed vacuum state and we show that the criteria based on triples of probabilities are more powerful than criteria based on pairs of probabilities only. Finally, Sec. VII contains a brief summary and conclusions.

II. SETUP DESCRIPTION

Consider the detection scheme illustrated in Fig. 1. The input signal impinges on an unbalanced beam splitter with transmittance T and reflectance $R = 1 - T$ and is split into two output modes A and B . Each output mode is measured with a photodetector that can discriminate the absence or presence of photons. Such click detector is described by a two-component POVM:

$$\hat{\Pi}_0 = |0\rangle\langle 0|, \quad \hat{\Pi}_1 = \hat{I} - |0\rangle\langle 0| \quad (1)$$

where $|0\rangle$ denotes the vacuum state. In practice, the detectors exhibit nonunit detection efficiency η . Detection with inefficient detectors is equivalent to transmission of the input state over a lossy channel \mathcal{L}_η with transmittance η , followed by detection with perfect detectors. A lossy channel with transmittance η transforms a coherent state $|\alpha\rangle$ onto an attenuated coherent state $|\sqrt{\eta}\alpha\rangle$. Thus, the criteria derived below for perfect detectors are equally valid also for detectors with nonunit detection efficiency η , because the lossy channel maps the set of all coherent states and their mixtures onto the same set. If the detection efficiencies of the two detectors D_A and D_B differ, $\eta_A \neq \eta_B$, then one only has to carefully calibrate the setup and use an effective beam splitter transmittance [39]:

$$\tilde{T} = \frac{\eta_A T}{\eta_A T + \eta_B (1 - T)}. \quad (2)$$

In what follows, we therefore focus on the case of perfect detectors.

With the measurement scheme in Fig. 1 one can record the number of clicks of detector D_A and detector D_B , and the number of coincidence counts of D_A and D_B for some total number of measurements N . In case of pulsed sources, each elementary detection can be triggered by a signal from the source. The measurements can be performed also for continuous-wave sources, for instance by recording the signals from the detectors with a time tagger. N elementary windows of width Δt can be defined within the total measurement time and for each detection window it can be decided from the recorded data whether a given detector clicked or not within that window.

For our purposes, it is convenient to consider the probability p_{AB} that none of the detectors D_A and D_B clicks, probability p_A that the detector D_A does not click (irrespective of the response of D_B), and probability p_B that the detector D_B does not click. These latter probabilities can be straightforwardly obtained from the probabilities of clicks of single detectors and the probability of coincidence clicks. For the input coherent state with complex amplitude α we get

$$p_A = e^{-T|\alpha|^2}, \quad p_B = e^{-(1-T)|\alpha|^2}, \quad p_{AB} = e^{-|\alpha|^2}. \quad (3)$$

More generally, for input state $\hat{\rho}$ the probability of no-click p_j is equal to the probability of vacuum in a state transmitted through a lossy quantum channel with specific transmittance η_j :

$$p_j = \langle 0 | \mathcal{L}_{\eta_j}(\hat{\rho}) | 0 \rangle, \quad (4)$$

where $\eta_A = T$, $\eta_B = 1 - T$, and $\eta_{AB} = 1$.

The Hanbury Brown–Twiss setup in Fig. 1 is the simplest case of photodetectors based on spatial or temporal multiplexing that can be used to efficiently probe quantum statistical properties of light and achieve partial photon number resolution with binary on-off detectors (1) [5,35,40–49]. In particular, arrays of photodetectors provide specific possibilities for probing the nonclassicality [5,7,8] and quantum non-Gaussianity [50–52] of light. There is an interesting connection between the unbalanced two-detector scheme in Fig. 1 and measurements with a balanced array of N binary click detectors (see Fig. 2). If we employ the balanced N -detector scheme, we can split the detectors into two groups. The first group is formed by k detectors and the other is formed by the remaining $N - k$ detectors. The probability p_A can then be defined as the probability that none of the k detectors in the first group clicks, irrespective of the response of the detectors in the other group. The probability p_B can be defined similarly as the probability that none of the $N - k$ detectors in the other group clicks, irrespective of the response of the detectors in the first group. Finally, p_{AB} can be defined as the probability that none of the N detectors clicks. With this assignment we obtain the measurement probabilities for the effective unbalanced two-detector scheme with $T = k/N$.

More generally, the measurement with the balanced N -detector scheme enables us to simultaneously estimate probabilities of no-clicks for N transmittances $T = k/N$, $k = 1, \dots, N$ [52]. In principle, all these data can be used simultaneously to characterize the nonclassicality of the measured state, extending the scenario considered in the present paper. The setup where the signal is evenly split among N detectors

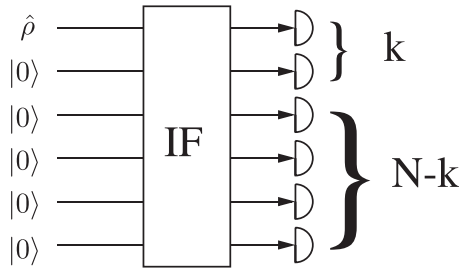


FIG. 2. Connection between an unbalanced two-detector scheme and a balanced detector array scheme where the input signal is evenly split by an interferometer IF among N detectors that can distinguish the presence and absence of photons. If we divide the detectors into two groups containing k and $N - k$ detectors, respectively, then we can measure the probabilities p_A , p_B , and p_{AB} for effective transmittance $T = k/N$. A balanced Hanbury Brown–Twiss setup with $T = \frac{1}{2}$ represents the simplest instance of the balanced detector array with $N = 2$. See text for details.

is actually very degenerate. We can imagine an unbalanced setup with N binary on-off detectors, where the effective transmittance of a path that leads from the input to the j th detector reads $T_j = 2^{-j}/(1 - 2^{-N})$, so that the transmittances sum up to 1. By considering various groups of detectors, we can simultaneously measure the probabilities of no-clicks (4) for $2^N - 1$ different nonzero transmittances. However, such approach may require extremely precise calibration of the transmittances to fully and correctly utilize all the available measurement channels.

III. CONVEX HULL CONSTRUCTION

The probabilities of no-clicks (3) specify a point in a three-dimensional space, and we can define a corresponding vector:

$$\vec{r} = [p_A, p_B, p_{AB}]. \quad (5)$$

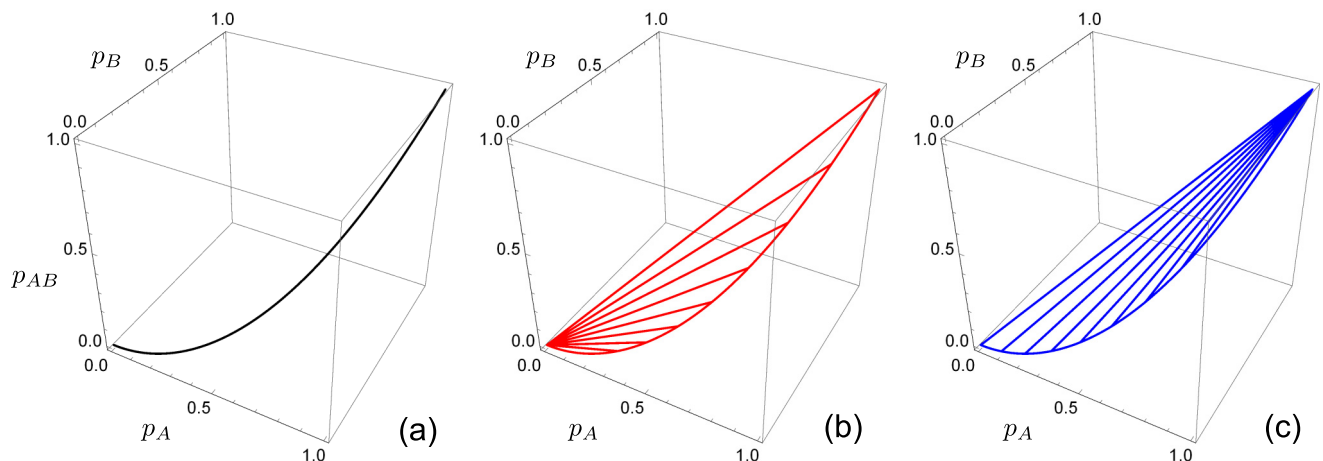


FIG. 3. (a) Three-dimensional curve (10) of coherent-state probability triples $[p_A, p_B, p_{AB}]$ for an unbalanced Hanbury Brown–Twiss detection scheme with $T = 1/3$. (b) The lower boundary of the convex hull of the curve is a surface formed by straight lines that connect the point $[0,0,0]$ with all other points of the curve. (c) Similarly, the upper boundary of the convex hull is a surface formed by straight lines that connect the point $[1,1,1]$ with all other points of the curve [36].

The points in this three-dimensional space that correspond to coherent states form a curve that is parametrically described by Eq. (3), where $|\alpha| \in [0, \infty)$ [see Fig. 3(a)]. Consider now an arbitrary state $\hat{\rho}$ and the associated probabilities \vec{r}_ρ . For any state $\hat{\sigma}$ that is a coherent state or a convex mixture of coherent states, the point \vec{r}_σ lies in the convex hull of the curve (3), because the probability triplet \vec{r}_σ can be expressed as a convex mixture of the points (3):

$$\vec{r}_\sigma = \int_0^\infty P(|\alpha|) [e^{-T|\alpha|^2}, e^{-(1-T)|\alpha|^2}, e^{-|\alpha|^2}] d|\alpha|, \quad (6)$$

where $P(|\alpha|)$ denotes probability distribution. Conversely, if the point \vec{r}_ρ does not belong to the convex hull of the curve (3), then the state $\hat{\rho}$ is nonclassical. Therefore, to establish a nonclassicality criterion based on the triplet of probabilities p_A , p_B , and p_{AB} , we need to construct the convex hull of the set (3) [11]. Recall that the convex hull of a set S is the smallest convex set that contains S . The convex hull is fully characterized by its boundary and in what follows we focus on the construction of this boundary.

Without loss of generality, we shall assume $T < 1/2$. Let us first consider just the pair of probabilities $[p_A, p_B]$. All pairs of probabilities p_A and p_B that can be observed for classical states form a two-dimensional convex set that is bounded by the curve $p_B = p_A^{(1-T)/T}$ and by the line $p_B = p_A$ [6]. We thus obtain a two-dimensional convex set of probability pairs p_A and p_B compatible with classical states [6,12] [see Fig. 4(a)]. The convexity of this two-dimensional set is ensured by the fact that $(1 - T)/T > 1$ for $T < 1/2$. If the measured pair of probabilities $[p_A, p_B]$ lies outside this set, then the state is certified to be nonclassical.

Suppose now that the pair $[p_A, p_B]$ is compatible with classical states and let us take into account the third probability p_{AB} . In order to decide whether the point $[p_A, p_B, p_{AB}]$ lies in the convex hull of (3) or not, we can compare the actual value of p_{AB} with the maximum and minimum values of p_{AB} that can be obtained, for given values of p_A and p_B , by measurements on classical states [11]. The resulting dependence of

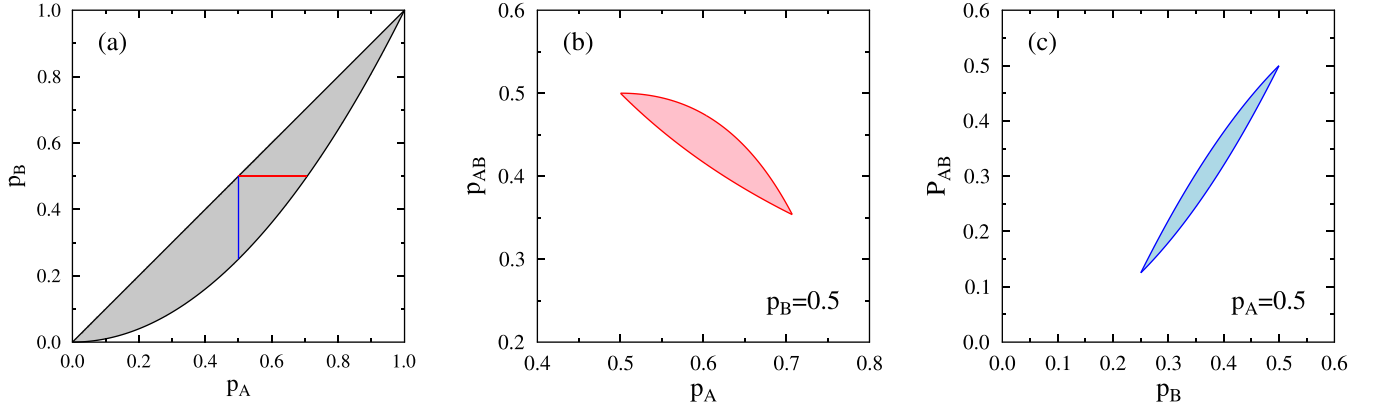


FIG. 4. The area of probability pairs $[p_A, p_B]$ that can be obtained for classical states when $T = 1/3$ (a) is plotted together with two two-dimensional cuts through the convex hull of probability triples (14) obtained at $p_B = 0.5$ (b) and $p_A = 0.5$ (c).

maximum and minimum values of p_{AB} on p_A and p_B specifies two surfaces that form two parts of the boundary of the convex hull of (3). We can thus succinctly express the conditions that a given triplet $[p_A, p_B, p_{AB}]$ lies in the convex hull of (3) as follows:

$$p_A^{1/T-1} \leq p_B \leq p_A \quad (7)$$

and

$$p_{AB,\min}(p_A, p_B) \leq p_{AB} \leq p_{AB,\max}(p_A, p_B). \quad (8)$$

The lower and upper bounds $p_{AB,\min}$ and $p_{AB,\max}$, which are functions of p_A and p_B , can be found using the results of Ref. [36] where the problem of constructing the convex hull of a curve was addressed by a geometric approach for so-called curves with totally positive torsion (see also Refs. [37,38]).

Consider a three-dimensional curve $\vec{r}(x)$ parametrized by $x \in [0, 1]$. According to Ref. [36] the curve is said to have totally positive torsion if all the leading principal minors of the matrix

$$C = \left[\frac{d\vec{r}}{dx}, \frac{d^2\vec{r}}{dx^2}, \frac{d^3\vec{r}}{dx^3} \right] \quad (9)$$

are positive for all $x \in (0, 1)$.

Let us define $x = \exp(-|\alpha|^2)$; hence $x \in [0, 1]$, where we include also the point that is obtained in the asymptotic limit $|\alpha| \rightarrow \infty$. The curve (3) becomes parametrized as

$$\vec{r} = [x^T, x^{1-T}, x] \quad (10)$$

and a straightforward calculation yields

$$C = \begin{bmatrix} Tx^{T-1} & T(T-1)x^{T-2} & T(1-T)(2-T)x^{T-3} \\ (1-T)x^{-T} & T(T-1)x^{-T-1} & T(1-T)(1+T)x^{-T-2} \\ 1 & 0 & 0 \end{bmatrix}. \quad (11)$$

It is easy to verify that all the leading principal minors of this matrix are positive for all $x \in (0, 1)$ and all $T \in (0, 1/2)$. Therefore, the results reported in Ref. [36] are directly applicable. Specifically, it is shown in Ref. [36] that the lower boundary $p_{AB,\min}$ of the convex hull is formed by a surface that consists of straight lines that connect the end point $[0,0,0]$ with all the other points on the curve [see Fig. 3(b)]. A parametric description of this surface reads

$$p_A = tx^T, \quad p_B = tx^{1-T}, \quad p_{AB} = tx, \quad (12)$$

where $t \in [0, 1]$ and $x \in [0, 1]$. Similarly, the upper boundary $p_{AB,\max}$ of the convex hull is formed by straight lines that connect the end point $[1,1,1]$ with all the other points on the curve [see Fig. 3(c)]. A parametric description of this surface is given by

$$\begin{aligned} p_A &= tx^T + 1 - t, \\ p_B &= tx^{1-T} + 1 - t, \\ p_{AB} &= tx + 1 - t, \end{aligned} \quad (13)$$

where again $t \in [0, 1]$ and $x \in [0, 1]$.

The boundaries (12) and (13) together with the inequalities (7) and (8) establish tight criteria of nonclassicality based on probability triples $[p_A, p_B, p_{AB}]$ in the sense that for any probability triple we either find that it is compatible with some classical state (when it belongs to the convex hull) or we conclusively certify the nonclassicality of the state (when it lies outside the convex hull). In the following sections we discuss the structure of the boundary surfaces (12) and (13) in more details and provide explicit expressions for the functions $p_{AB,\min}$ and $p_{AB,\max}$, where possible.

IV. CRITERIA FOR THE CASE $T = 1/3$

In this section we consider the specific case $T = 1/3$, for which the treatment becomes particularly simple. For $T = 1/3$, the formula (3) becomes

$$p_A = x^{1/3}, \quad p_B = x^{2/3}, \quad p_{AB} = x, \quad x \in [0, 1]. \quad (14)$$

As discussed in Sec. III, the surface of minimal values of p_{AB} is formed by straight lines connecting the point $[0,0,0]$ and the

points $[x^{1/3}, x^{2/3}, x]$. On inserting $T = 1/3$ into the general parametric representation (12) of this surface, we obtain

$$p_A = tx^{1/3}, \quad p_B = tx^{2/3}, \quad p_{AB} = tx, \quad (15)$$

where $t \in [0, 1]$ and $x \in [0, 1]$. The parameters t and x can be eliminated, which yields an explicit formula for $p_{AB, \min}$ as a function of p_A and p_B :

$$p_{AB, \min} = \frac{p_B^2}{p_A}. \quad (16)$$

This surface is plotted in Fig. 3(b).

We can crosscheck that the surface (16) is indeed a part of the boundary of the convex hull of (14) by investigating the shape of this surface. Specifically, we can determine the surface curvature by looking at the eigenvalues of the matrix of second derivatives of $p_{AB, \min}$:

$$M = \begin{bmatrix} \frac{\partial^2 p_{AB}}{\partial p_A^2} & \frac{\partial^2 p_{AB}}{\partial p_A \partial p_B} \\ \frac{\partial^2 p_{AB}}{\partial p_A \partial p_B} & \frac{\partial^2 p_{AB}}{\partial p_B^2} \end{bmatrix}. \quad (17)$$

For the function (16) we explicitly get

$$M_{\downarrow} = \begin{bmatrix} \frac{2p_B^2}{p_A^3} & -\frac{2p_B}{p_A^2} \\ -\frac{2p_B}{p_A^2} & \frac{2}{p_A} \end{bmatrix}. \quad (18)$$

One eigenvalue of M_{\downarrow} is equal to zero, which is expected because the surface is formed by lines. The other eigenvalue is positive, which confirms that this surface has the required cup shape \cup and forms the bottom part of the boundary of the convex hull of (14), as already proved in Ref. [36].

As discussed in Sec. III, the surface of maximal values of p_{AB} is constructed similarly as a set of straight lines that connect the point $[1, 1, 1]$ and the points $[x^{1/3}, x^{2/3}, x]$ [36]. On inserting $T = 1/3$ into Eq. (13) we get the parametric representation of this surface:

$$p_A = tx^{1/3} + 1 - t, \quad p_B = tx^{2/3} + 1 - t, \quad p_{AB} = tx + 1 - t. \quad (19)$$

After some algebra, we can eliminate the parameters t and x and express $p_{AB, \max}$ as a function of p_A and p_B :

$$p_{AB, \max} = p_B - \frac{(p_A - p_B)^2}{1 - p_A}. \quad (20)$$

This surface is plotted in Fig. 3(c). Similarly as before, we can characterize the shape of the surface (20) by calculating the matrix of second derivatives (17), which yields

$$M_{\uparrow} = \begin{bmatrix} -\frac{2(1 - p_B)^2}{(1 - p_A)^3} & \frac{2(1 - p_B)}{(1 - p_A)^2} \\ \frac{2(1 - p_B)}{(1 - p_A)^2} & -\frac{2}{1 - p_A} \end{bmatrix}. \quad (21)$$

One eigenvalue of M_{\uparrow} is zero and the other is negative. This confirms that the surface (20) has the cap shape \cap and forms the upper part of the boundary of the convex hull of (14), in agreement with the results of Ref. [36]. Note that the two

surfaces (16) and (20) are connected at the boundary curve $[x^{1/3}, x^{2/3}, x]$, $x \in [0, 1]$ and also at the boundary line $[t, t, t]$, $t \in [0, 1]$.

The gray area in Fig. 4(a) represents a top view on the convex hull of probability triples (14). To further visualize the convex hull, we plot in Figs. 4(b) and 4(c) two-dimensional cuts through this three-dimensional set. The upper and lower boundaries in Figs. 4(b) and 4(c) are given by Eqs. (20) and (16), respectively.

V. GENERALIZATION TO ARBITRARY T

Here we analyze the lower and upper boundaries $p_{AB, \min}$ and $p_{AB, \max}$ for arbitrary $T < 1/2$. Let us first consider the lower bound $p_{AB, \min}$, where an explicit analytical expression can be obtained for any T . Parametric description of the surface $p_{AB, \min}$ is given by Eq. (12). The parameters t and x can be eliminated, which yields an explicit expression for $p_{AB, \min}$:

$$p_{AB, \min} = \left(\frac{p_B^{1-T}}{p_A^T} \right)^{\frac{1}{1-2T}}. \quad (22)$$

The matrix M of second derivatives, defined in Eq. (17), reads

$$M_{\downarrow} = \frac{T(1-T)}{(1-2T)^2} \left(\frac{p_B^{1-T}}{p_A^T} \right)^{\frac{1}{1-2T}} \begin{bmatrix} \frac{1}{p_A^2} & -\frac{1}{p_A p_B} \\ -\frac{1}{p_A p_B} & \frac{1}{p_B^2} \end{bmatrix}. \quad (23)$$

Similarly as for the special case $T = 1/3$ we find that one eigenvalue of M_{\downarrow} is zero while the other is positive, which confirms that the surface is convex and has the required cup shape \cup .

The situation becomes slightly more complicated for the upper bound $p_{AB, \max}$. We reproduce here for convenience the parametric description of this surface, which is given by Eq. (13):

$$\begin{aligned} p_A &= tx^T + 1 - t, \\ p_B &= tx^{1-T} + 1 - t, \\ p_{AB} &= tx + 1 - t. \end{aligned} \quad (24)$$

By combining formulas for p_A and p_B we obtain the equation for parameter x :

$$\frac{1 - p_A}{1 - p_B} = \frac{1 - x^T}{1 - x^{1-T}}. \quad (25)$$

Generally, this equation can be solved only numerically. If T is a rational number, then (25) can be transformed into a polynomial equation. In particular, for $T = 1/3$ Eq. (25) becomes a linear equation for $x^{1/3}$, which explains why we can obtain an explicit analytical formula for $p_{AB, \max}$ for this particular transmittance. If we experimentally determine the probabilities p_A , p_B , and p_{AB} then we can numerically solve Eq. (25) for x and subsequently determine t from the parametric expression for p_A . Finally, we can calculate the upper bound on p_{AB} as $p_{AB, \max} = xt + 1 - t$.

As discussed in Sec. III, the proof that Eq. (24) represents a part of the boundary of the convex hull of the curve (3) is provided in Ref. [36] for the general class of curves with totally

positive torsion. Nevertheless, for completeness we provide here an analysis of the curvature of the surface (24), which provides an independent confirmation of the validity of this boundary construction. We make use of standard techniques from differential geometry [53] and calculate the normal vector to the parametric surface (24) and its two curvatures. In what follows we will extensively utilize the probability vector \vec{r} , which now depends on t and x :

$$\vec{r} = \begin{bmatrix} tx^T + 1 - t \\ tx^R + 1 - t \\ tx^{R+T} + 1 - t \end{bmatrix}. \quad (26)$$

Here $R = 1 - T$ and it will be convenient to keep R explicitly in the definition of \vec{r} . A normal vector to the parametric surface (24) can be constructed as

$$\vec{n} = \frac{1}{w} \frac{\partial \vec{r}}{\partial t} \times \frac{\partial \vec{r}}{\partial x}, \quad (27)$$

where

$$w = \left| \frac{\partial \vec{r}}{\partial t} \times \frac{\partial \vec{r}}{\partial x} \right| \quad (28)$$

is a positive normalization factor. On inserting the explicit expression (26) for vector \vec{r} into Eq. (27) we get

$$\vec{n} = \frac{t}{wx} \begin{bmatrix} x^R(R - x^T + Tx) \\ x^T(x^R - T - Rx) \\ Tx^T(1 - x^R) - Rx^R(1 - x^T) \end{bmatrix}. \quad (29)$$

Recall that we assume that $T < 1/2$. The third component of the vector \vec{n} is then positive. We can rewrite this component as

$$n_3 = \frac{TRt}{w} \left[\frac{1 - x^R}{Rx^R} - \frac{1 - x^T}{Tx^T} \right]. \quad (30)$$

Consider the function

$$f(x, z) = \frac{1 - x^z}{zx^z} \quad (31)$$

where $z \in (0, 1)$. We have

$$\frac{\partial f(x, z)}{\partial z} = \frac{x^{-z}}{z^2} (x^z - 1 - z \ln x). \quad (32)$$

If we set $a = -z \ln x > 0$ and use the inequality $e^{-a} > 1 - a$ valid for all positive a , we can conclude that the partial derivative (32) is positive. Since we assume that $R > T$, this implies that n_3 is positive.

The first fundamental form that characterizes the surface (24) is specified by parameters [53]

$$E = \frac{\partial \vec{r}}{\partial t} \cdot \frac{\partial \vec{r}}{\partial t}, \quad F = \frac{\partial \vec{r}}{\partial t} \cdot \frac{\partial \vec{r}}{\partial x}, \quad G = \frac{\partial \vec{r}}{\partial x} \cdot \frac{\partial \vec{r}}{\partial x}. \quad (33)$$

The second fundamental form is characterized by

$$L = \frac{\partial^2 \vec{r}}{\partial t^2} \cdot \vec{n}, \quad M = \frac{\partial^2 \vec{r}}{\partial t \partial x} \cdot \vec{n}, \quad N = \frac{\partial^2 \vec{r}}{\partial x^2} \cdot \vec{n}. \quad (34)$$

After some algebra we find that $L = 0$ and $M = 0$, which is consistent with the fact that the studied surface is formed by

straight lines and one of its principal curvatures vanishes. The other principal curvature reads

$$\kappa = \frac{EN}{EG - F^2}. \quad (35)$$

Since

$$\frac{E}{EG - F^2} > 0 \quad (36)$$

by definition [53], it suffices to study the sign of N to determine the shape of the surface. Explicitly, we have

$$N = \frac{R^2 T^2 t^2}{wx^2} (1 + x^R)(1 + x^T) \left[\frac{1 - x^R}{R(1 + x^R)} - \frac{1 - x^T}{T(1 + x^T)} \right]. \quad (37)$$

We proceed similarly as before when we have analyzed the sign of n_3 . Let us define a new function

$$g(x, z) = \frac{1 - x^z}{z(1 + x^z)} \quad (38)$$

and analyze its partial derivative

$$\frac{\partial g(x, z)}{\partial z} = \frac{x^{2z} - 1 - 2zx^z \ln x}{z^2(1 + x^z)^2}. \quad (39)$$

Upon making substitution $a = -z \ln x \geq 0$ we can rewrite the term in the numerator of Eq. (39) as

$$e^{-2a} - 1 + 2ae^{-a} = 2e^{-a}[a - \sinh a] \leq 0, \quad (40)$$

which holds for all $a \geq 0$. We have thus proved that the partial derivative (39) is negative for all $x \in (0, 1)$ and $z > 0$. Since we assume that $T < 1/2$, hence $R > T$, this implies that

$$\frac{1 - x^R}{R(1 + x^R)} < \frac{1 - x^T}{T(1 + x^T)}. \quad (41)$$

Therefore, $N < 0$ and the curvature (35) is negative. This confirms that the upper boundary surface has the cap shape \cap .

For the sake of completeness we note that the convex hull of the set (3) can be equivalently characterized by its tangent planes. Each tangent plane corresponds to a nonclassicality witness. The nonclassicality witnesses are similar in spirit to entanglement witnesses or Bell inequalities [12,54–56], because in all cases the goal is to prove that certain states lie outside some convex set. Specifically, we can consider a witness

$$W = n_1 p_A + n_2 p_B + n_3 p_{AB} \quad (42)$$

associated with the unit normal vector \vec{n} and seek the maximum of W over all classical states. It suffices to maximize W over the coherent states, which means that we need to find the maximum of

$$W = n_1 x^T + n_2 x^{1-T} + n_3 x, \quad x \in [0, 1]. \quad (43)$$

We need to identify potential local extrema of W by solving

$$T n_1 x^{T-1} + (1 - T) n_2 x^{-T} + n_3 = 0. \quad (44)$$

In addition, we also have to consider the boundary points $x = 0$ and 1 . The roots of (44) can easily be found numerically. For $T = 1/3$ this equation becomes equivalent to a quadratic

equation for $x^{1/3}$. More generally, the function on the left-hand side of Eq. (44) has at most a single local extremum in the interval (0,1), hence Eq. (44) has at most two roots in this interval. The construction of the boundary surface (24) implies that the tangent plane associated with the normal vector (29) touches the surface along a whole line and passes through the point [1,1,1]. Therefore, the maximum value of W is achieved at $x = 1$ and we obtain a nonclassicality condition

$$n_1 p_A + n_2 p_B + n_3 p_{AB} > n_1 + n_2 + n_3 \quad (45)$$

valid for normal vectors (29).

Using Eq. (27) we can determine also the normal vector to the lower boundary surface (12):

$$\vec{m} = \frac{1}{w_m} \begin{bmatrix} T x^{1-T} \\ (T-1)x^T \\ 1-2T \end{bmatrix}, \quad (46)$$

where

$$w_m = [T^2 x^{2-2T} + (1-T)^2 x^{2T} + (1-2T)^2]^{1/2}. \quad (47)$$

We assume $T < 1/2$, hence $m_3 > 0$. The associated tangent planes again touch the surface along straight lines and pass through the point [0,0,0]. Therefore, $m_1 p_A + m_2 p_B + m_3 p_{AB}$ is bounded by zero and the state is certified as nonclassical if

$$m_1 p_A + m_2 p_B + m_3 p_{AB} < 0 \quad (48)$$

for the normal vectors (46). We have cross-checked the nonclassicality thresholds (45) and (48) by numerical calculations and we have obtained full agreement with analytical results. The nonclassicality witnesses (45) and (48) are tight by construction, because the associated tangent planes touch the surface of the convex hull along straight lines.

VI. APPLICATION TO SQUEEZED VACUUM STATES

Here we show that the above derived nonclassicality criteria can be used to detect nonclassicality of the single-mode squeezed vacuum state

$$|\psi\rangle = \frac{1}{\sqrt{\cosh s}} \sum_{n=0}^{\infty} (-\tanh s)^n \frac{\sqrt{(2n)!}}{2^n n!} |2n\rangle, \quad (49)$$

where s denotes the squeezing constant and $|n\rangle$ denotes Fock states. The state (49) is Gaussian with zero mean values of quadrature operators, hence it is fully characterized by its covariance matrix

$$\gamma_{SV} = \begin{pmatrix} e^{-2s} & 0 \\ 0 & e^{2s} \end{pmatrix}, \quad (50)$$

that collects the variances and covariances of quadrature operators \hat{x} and \hat{p} . The covariance matrix (50) is normalized such that it is equal to the identity matrix I for the vacuum state. In order to calculate the probabilities p_A and p_B we also need to consider a state transmitted through a lossy channel with certain transmittance η . The lossy channel preserves the Gaussian form of the state, and the covariance matrix of the output state is given by

$$\gamma_{\text{out}} = \eta \gamma_{\text{in}} + (1-\eta)I. \quad (51)$$

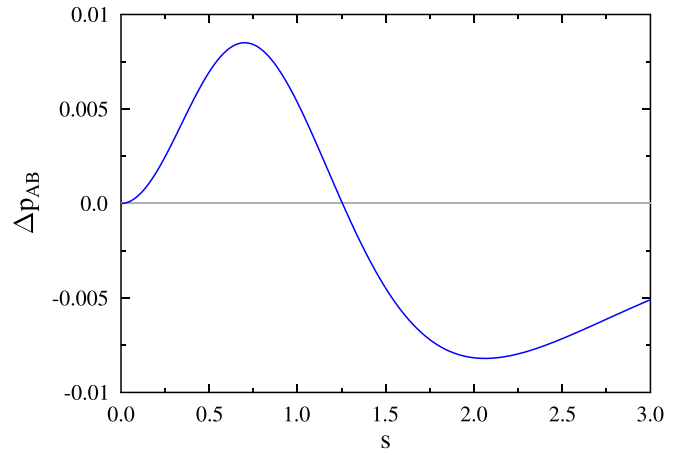


FIG. 5. Certification of nonclassicality of a single-mode squeezed vacuum state with squeezing constant s via the nonclassicality condition $p_{AB} > p_{AB,\max}$ for $T = 1/3$. We set $T = 1/3$, hence $p_{AB,\max}$ is given by Eq. (20). Nonclassicality is confirmed in the region where $\Delta p_{AB} = p_{AB} - p_{AB,\max} > 0$.

For a single-mode Gaussian state $\hat{\rho}$ with zero mean value of quadratures and covariance matrix γ , the vacuum probability $p_0 = \langle 0|\hat{\rho}|0\rangle$ can be expressed in terms of the covariance matrix as follows:

$$p_0 = \frac{2}{\sqrt{\det(\gamma + I)}}. \quad (52)$$

This formula can be easily derived with the use of the Husimi Q function of the state, $Q(\alpha) = \pi^{-1} \langle \alpha|\hat{\rho}|\alpha\rangle$, where $|\alpha\rangle$ denotes a coherent state with amplitude α , because $p_0 = \pi Q(0)$. The Q function of a Gaussian state with zero mean is a Gaussian distribution centered on the origin with covariance matrix $\frac{1}{4}(\gamma + I)$.

Using Eq. (52) we obtain the following expressions for the probabilities p_A , p_B , and p_{AB} associated with the measurement of the single-mode squeezed state (49) with the setup in Fig. 1:

$$\begin{aligned} p_A &= \frac{1}{\sqrt{1 + T(2-T)\sinh^2 s}}, \\ p_B &= \frac{1}{\sqrt{1 + (1-T^2)\sinh^2 s}}, \\ p_{AB} &= \frac{1}{\cosh s}. \end{aligned} \quad (53)$$

In Fig. 5 we plot the dependence of $\Delta p_{AB} = p_{AB} - p_{AB,\max}$ on s for $T = 1/3$. We can see that the nonclassicality of the squeezed state (49) can be certified for all squeezing constants up to $s \approx 1.25$. By contrast, the nonclassicality of certain squeezed states cannot be revealed if one considers only pairs of the detected probabilities. Assume $T < 1/2$, as before. Using a pair of probabilities, the state is certified to be nonclassical if at least one of the following inequalities is violated [6]:

$$p_B \geq p_A^{1/T-1}, \quad p_{AB} \geq p_A^{1/T}, \quad p_{AB} \geq p_B^{1/(1-T)}. \quad (54)$$

These nonclassicality conditions directly follow from the parametrization $[x^T, x^{1-T}, x]$ of the set of coherent-state probabilities and from the fact that the function x^k is convex

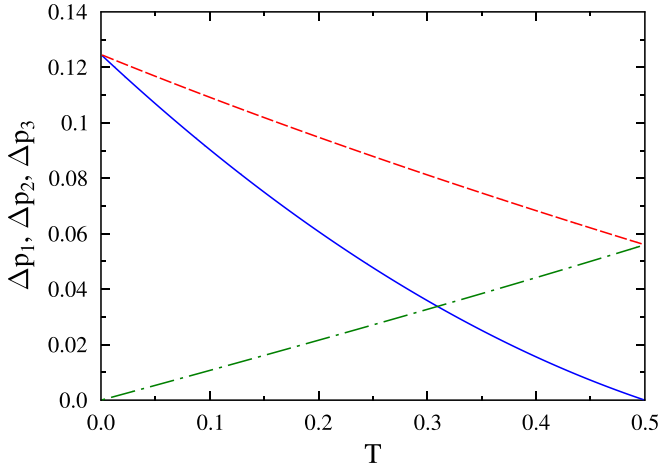


FIG. 6. Test of nonclassicality of a single-mode squeezed vacuum with criteria (56). The quantities Δp_1 (solid blue line), Δp_2 (red dashed line), and Δp_3 (green dot-dashed line) are plotted in dependence on T for $s = 0.5$. Nonclassicality of the state cannot be detected with any of these three criteria.

for $k \geq 1$ [see also the discussion in Sec. III and Fig. 4(a)]. Besides the lower bounds (54), one could also consider the corresponding upper bounds:

$$p_{AB} \leq p_B \leq p_A. \quad (55)$$

However, these inequalities are satisfied by all physical states, therefore they do not represent useful nonclassicality criteria.

As an example, we have evaluated all three criteria (54) for fixed squeezing $s = 0.5$ and variable transmittance T . In Fig. 6 we plot the resulting quantities

$$\begin{aligned} \Delta p_1 &= p_B - p_A^{1/T-1}, \\ \Delta p_2 &= p_{AB} - p_A^{1/T}, \\ \Delta p_3 &= p_{AB} - p_B^{1/(1-T)} \end{aligned} \quad (56)$$

as functions of T . We can see that the criteria (54) cannot detect nonclassicality of the squeezed vacuum state with $s = 0.5$, while the criterion plotted in Fig. 5 clearly detects this state as nonclassical. This shows that the criteria based on all three probabilities p_A , p_B , and p_{AB} are strictly stronger than criteria based on pairs of probabilities only.

For completeness, in Fig. 7 we plot the dependence of Δp_{AB} on T for a fixed squeezing strength s . It can be seen that for $s = 0.75$ the nonclassicality of the squeezed state can be certified for any $0 < T < \frac{1}{2}$, and the value of Δp_{AB} is finite and positive for T arbitrary close to $\frac{1}{2}$. At the point $T = \frac{1}{2}$ there is thus a discontinuity, because for a precisely balanced beam splitter the probability p_{AB} achievable by classical states is upper bounded only by the trivial inequality $p_{AB} < p_A$, and $p_B = p_A$ due to symmetry. In order to investigate the behavior of the nonclassicality criterion $p_{AB} \leq p_{AB,\max}$ for the squeezed vacuum state (49) in the vicinity of $T = \frac{1}{2}$, we can expand both sides of Eq. (25) in Taylor series in variable $\epsilon = \frac{1}{2} - T$. By comparing the leading terms proportional to ϵ , we find that in the vicinity of $T = \frac{1}{2}$ the parameter x is determined by the

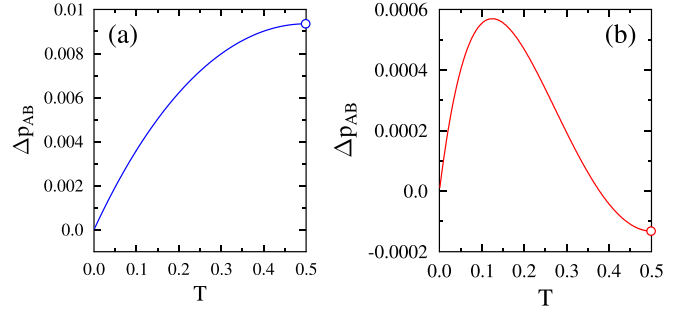


FIG. 7. Dependence of the nonclassicality test $\Delta p_{AB} = p_{AB} - p_{AB,\max}$ on beam splitter transmittance T is plotted for single-mode squeezed vacuum states with two values of squeezing $s = 0.75$ (a) and $s = 1.25$ (b). As discussed in the main text, a discontinuity occurs at the point $T = \frac{1}{2}$, where the setup becomes degenerate and $p_A = p_B$ holds exactly. For example, for $s = 0.75$ we obtain $\Delta p_{AB} = p_{AB} - p_A \approx -0.0422$ at the exact degeneracy $T = \frac{1}{2}$.

following equation:

$$\frac{\sqrt{x} \ln x}{\sqrt{x} - 1} = \frac{4 \sinh^2 s}{(4 + 3 \sinh^2 s)(\sqrt{4 + 3 \sinh^2 s} - 2)}. \quad (57)$$

This equation has a single root in the interval $[0,1]$, and this root is strictly positive for $s \neq 0$. Explicit calculations based on Eq. (13) confirm that the resulting upper bound $p_{AB,\max}$ is strictly smaller than p_A . All this breaks down for the perfectly balanced scheme with $T = \frac{1}{2}$, where the degeneracy deletes the information that otherwise allows us to establish such a strict upper bound on p_{AB} .

From the experimental point of view, it is not desirable to operate in the close vicinity of $T = \frac{1}{2}$, because in such case the statistical uncertainties of estimations of p_A and p_B could significantly affect the applicability of the nonclassicality criteria (7) and (8), and the measurement of the no-click probabilities as well as the calibration of the value of T would have to be very precise to correctly sample the tiny difference between p_A and p_B .

VII. CONCLUSIONS

We have derived tight nonclassicality criteria that fully exploit information that can be extracted from an unbalanced Hanbury Brown–Twiss measurement scheme with binary click detectors. Our nonclassicality criteria are based on complete characterization of the three-dimensional convex set of probabilities achievable with classical states, which is provided by explicit description of the boundary of this set. An equivalent complementary formulation of the nonclassicality criteria based on nonclassicality witnesses was also considered and we were able to obtain explicit tight bounds on these witnesses, based on geometric considerations. The criteria discussed in the present paper conclusively certify nonclassicality of certain states. However, when some state is not identified as nonclassical by the present criteria, the situation is inconclusive and one cannot claim that the state is classical. For instance, consider a state the nonclassicality of which is fully encoded into coherence properties, i.e., phase

shifts of Fock states. As an example take a state generated by Kerr interaction from a coherent state. Such state would exhibit Poisson photon number statistics, yet it could be highly nonclassical.

Before closing up, let us briefly discuss imperfections that can influence the considered measurement. We have already argued in Sec. II that the obtained nonclassicality criteria are fully valid also for detectors with limited detection efficiency $\eta < 1$. Additional effects that can influence the observed click statistics include dark counts and afterpulses. These two effects can be largely eliminated in gated detection schemes with pulsed sources, where the measurement is always activated only in a short time window that corresponds to the arrival of the measured optical pulse at the detectors. In situations where the effects of afterpulses and dark counts cannot be fully suppressed, they should be carefully characterized. One can then attempt to recover the true click statistics from the measured statistics, by correcting for the effects of dark counts and afterpulses.

In our derivations we have assumed that a single spatiotemporal and polarization mode is detected. The single-mode condition can be imposed by polarization, spatial and spectral filtering, which can however introduce additional losses that can make it difficult to observe the nonclassicality of the probed state. If the effective splitting ratio $T : R$ is the same for all modes involved, then our criteria hold even for broadband multimode detection. This straightforwardly follows from the factorized form of multimode coherent states

$|\alpha\rangle = |\alpha_1\rangle|\alpha_2\rangle \cdots |\alpha_k\rangle \cdots |\alpha_K\rangle$ where K denotes the total number of modes. If T is the same for all modes, we have for the input multimode coherent state

$$\begin{aligned} p_A &= \prod_{j=1}^K e^{-T|\alpha_j|^2}, \\ p_B &= \prod_{j=1}^K e^{-(1-T)|\alpha_j|^2}, \\ p_{AB} &= \prod_{j=1}^K e^{-|\alpha_j|^2}. \end{aligned} \quad (58)$$

This is fully equivalent to the single-mode expression (3), where we only need to set $|\alpha|^2 = \sum_{j=1}^K |\alpha_j|^2$.

Our findings provide criteria and witnesses available for verification of nonclassical character of quantum states of light. It would be interesting to further extend this analysis to certification of other state properties, such as quantum non-Gaussianity [34,39,52,57]. However, if we extend the set of pure extremal states from coherent states to all pure Gaussian states, the analysis becomes much more involved. These investigations are therefore left for future work.

ACKNOWLEDGMENT

The author acknowledges support by the Czech Science Foundation under Grant No. GA21-18545S.

-
- [1] H. J. Kimble, M. Dagenais, and L. Mandel, Photon antibunching in resonance fluorescence, *Phys. Rev. Lett.* **39**, 691 (1977).
 - [2] P. Grangier, G. Roger, and A. Aspect, Experimental evidence for a photon anticorrelation effect on a beam splitter: A new light on single-photon interferences, *Europhys. Lett.* **1**, 173 (1986).
 - [3] M. D. Reid and D. F. Walls, Violations of classical inequalities in quantum optics, *Phys. Rev. A* **34**, 1260 (1986).
 - [4] D. N. Klyshko, Observable signs of nonclassical light, *Phys. Lett. A* **213**, 7 (1996).
 - [5] J. Sperling, W. Vogel, and G. S. Agarwal, Sub-binomial light, *Phys. Rev. Lett.* **109**, 093601 (2012).
 - [6] R. Filip and L. Lachman, Hierarchy of feasible nonclassicality criteria for sources of photons, *Phys. Rev. A* **88**, 043827 (2013).
 - [7] J. Sperling, W. R. Clements, A. Eckstein, M. Moore, J. J. Renema, W. S. Kolthammer, S. W. Nam, A. Lita, T. Gerrits, W. Vogel, G. S. Agarwal, and I. A. Walmsley, Detector-independent verification of quantum light, *Phys. Rev. Lett.* **118**, 163602 (2017).
 - [8] J. Sperling, A. Eckstein, W. R. Clements, M. Moore, J. J. Renema, W. S. Kolthammer, S. W. Nam, A. Lita, T. Gerrits, I. A. Walmsley, G. S. Agarwal, and W. Vogel, Identification of nonclassical properties of light with multiplexing layouts, *Phys. Rev. A* **96**, 013804 (2017).
 - [9] L. Lachman and R. Filip, Criteria for single photon sources with variable nonclassicality threshold, *New J. Phys.* **21**, 083012 (2019).
 - [10] J. Peřina, V. Michálek, and O. Haderka, Non-classicality of optical fields as observed in photocount and photon-number distributions, *Opt. Express* **28**, 32620 (2020).
 - [11] L. Innocenti, L. Lachman and R. Filip, Nonclassicality detection from few Fock-state probabilities, *npj Quantum Inf.* **8**, 30 (2022).
 - [12] V. S. Kovtoniuk, E. V. Stolyarov, O. V. Kliushnichenko, A. A. Semenov, Tight inequalities for nonclassicality of measurement statistics, [arXiv:2310.14263](https://arxiv.org/abs/2310.14263).
 - [13] C. T. Lee, Many-photon antibunching in generalized pair coherent states, *Phys. Rev. A* **41**, 1569 (1990).
 - [14] C. T. Lee, Higher-order criteria for nonclassical effects in photon statistics, *Phys. Rev. A* **41**, 1721 (1990).
 - [15] G. S. Agarwal and K. Tara, Nonclassical character of states exhibiting no squeezing or sub-Poissonian statistics, *Phys. Rev. A* **46**, 485 (1992).
 - [16] A. Miranowicz, M. Bartkowiak, X. Wang, Y. Liu, and F. Nori, Testing nonclassicality in multimode fields: A unified derivation of classical inequalities, *Phys. Rev. A* **82**, 013824 (2010).
 - [17] L. Rigovacca, C. Di Franco, B. J. Metcalf, I. A. Walmsley, and M. S. Kim, Nonclassicality criteria in multiport interferometry, *Phys. Rev. Lett.* **117**, 213602 (2016).
 - [18] P. Grünwald, Effective second-order correlation function and single-photon detection, *New J. Phys.* **21**, 093003 (2019).
 - [19] W. Vogel, Nonclassical states: An observable criterion, *Phys. Rev. Lett.* **84**, 1849 (2000).

- [20] T. Richter and W. Vogel, Nonclassicality of quantum states: A hierarchy of observable conditions, *Phys. Rev. Lett.* **89**, 283601 (2002).
- [21] J. Park, J. Zhang, J. Lee, S.-W. Ji, M. Um, D. Lv, K. Kim, and H. Nha, Testing nonclassicality and non-Gaussianity in phase space, *Phys. Rev. Lett.* **114**, 190402 (2015).
- [22] J. Park and H. Nha, Demonstrating nonclassicality and non-Gaussianity of single-mode fields: Bell-type tests using generalized phase-space distributions, *Phys. Rev. A* **92**, 062134 (2015).
- [23] M. Bohmann, E. Agudelo, and J. Sperling, Probing non-classicality with matrices of phase-space distributions, *Quantum* **4**, 343 (2020).
- [24] M. Bohmann and E. Agudelo, Phase-space inequalities beyond negativities, *Phys. Rev. Lett.* **124**, 133601 (2020).
- [25] J. Park, J. Lee, and H. Nha, Verifying single-mode nonclassicality beyond negativity in phase space, *Phys. Rev. Res.* **3**, 043116 (2021).
- [26] L. Innocenti, L. Lachman, and R. Filip, Coherence-based operational nonclassicality criteria, *Phys. Rev. Lett.* **131**, 160201 (2023).
- [27] M. Hillery, Nonclassical distance in quantum optics, *Phys. Rev. A* **35**, 725 (1987).
- [28] C. T. Lee, Measure of the nonclassicality of nonclassical states, *Phys. Rev. A* **44**, R2775 (1991).
- [29] J. K. Asbóth, J. Calsamiglia, and H. Ritsch, Computable measure of nonclassicality for light, *Phys. Rev. Lett.* **94**, 173602 (2005).
- [30] A. Miranowicz, K. Bartkiewicz, A. Pathak, J. Peřina, Y.-N. Chen, and F. Nori, Statistical mixtures of states can be more quantum than their superpositions: Comparison of nonclassicality measures for single-qubit states, *Phys. Rev. A* **91**, 042309 (2015).
- [31] B. Yadin, F. C. Binder, J. Thompson, V. Narasimhachar, M. Gu, and M. S. Kim, Operational resource theory of continuous-variable nonclassicality, *Phys. Rev. X* **8**, 041038 (2018).
- [32] A. Rivas and A. Luis, Nonclassicality of states and measurements by breaking classical bounds on statistics, *Phys. Rev. A* **79**, 042105 (2009).
- [33] R. Hanbury Brown and R. Q. Twiss, A Test of a New Type of Stellar Interferometer on Sirius, *Nature (London)* **178**, 1046 (1956).
- [34] M. Jeřek, I. Straka, M. Miřuda, M. Duřek, J. Fiurářek, and R. Filip, Experimental test of the quantum non-Gaussian character of a heralded single-photon state, *Phys. Rev. Lett.* **107**, 213602 (2011).
- [35] J. Řeháček, Z. Hradil, O. Haderka, J. Peřina Jr., and M. Hamar, Multiple-photon resolving fiber-loop detector, *Phys. Rev. A* **67**, 061801(R) (2003).
- [36] J. de Dios Pont, P. Ivanisvili, and J. Madrid, A new proof of the description of the convex hull of space curves with totally positive torsion, [arXiv:2201.12932](https://arxiv.org/abs/2201.12932).
- [37] S. Karlin and W. J. Studden, *Tchebycheff Systems: With Applications in Analysis and Statistics* (Interscience, New York, 1966).
- [38] M. G. Krein and A. A. Nudelman, *The Markov Moment Problem and Extremal Problems*, Translations of Mathematical Monographs Vol. 50 (American Mathematical Society, Providence, 1977).
- [39] J. Fiurářek, L. Lachman and R. Filip, Quantum non-Gaussianity criteria based on vacuum probabilities of original and attenuated state, *New J. Phys.* **23**, 073005 (2021).
- [40] H. Paul, P. Törmä, T. Kiss, and I. Jex, Photon chopping: New way to measure the quantum state of light, *Phys. Rev. Lett.* **76**, 2464 (1996).
- [41] K. Banaszek and I. A. Walmsley, Photon counting with a loop detector, *Opt. Lett.* **28**, 52 (2003).
- [42] D. Achilles, C. Silberhorn, C. Sliwa, K. Banaszek, and I. A. Walmsley, Fiber-assisted detection with photon number resolution, *Opt. Lett.* **28**, 2387 (2003).
- [43] M. J. Fitch, B. C. Jacobs, T. B. Pittman, and J. D. Franson, Photon-number resolution using time-multiplexed single-photon detectors, *Phys. Rev. A* **68**, 043814 (2003).
- [44] D. A. Kalashnikov, S. H. Tan, M. Chekhova, and L. A. Krivitsky, Accessing photon bunching with a photon number resolving multi-pixel detector, *Opt. Express* **19**, 9352 (2011).
- [45] F. Mattioli, Z. Zhou, A. Gaggero, R. Gaudio, R. Leoni, and A. Fiore, Photon-counting and analog operation of a 24-pixel photon number resolving detector based on superconducting nanowires, *Opt. Express* **24**, 9067 (2016).
- [46] J. Kröger, T. Ahrens, J. Sperling, W. Vogel, H. Stolz, and B. Hage, High intensity click statistics from a 10×10 avalanche photodiode array, *J. Phys. B* **50**, 214003 (2017).
- [47] D. Zhu, Q.-Y. Zhao, H. Choi, T.-J. Lu, A. E. Dane, D. Englund, and K. K. Berggren, A scalable multi-photon coincidence detector based on superconducting nanowires, *Nat. Nanotechnol.* **13**, 596 (2018).
- [48] J. Tiedau, E. Meyer-Scott, T. Nitsche, S. Barkhofen, T. J. Bartley, and C. Silberhorn, A high dynamic range optical detector for measuring single photons and bright light, *Opt. Express* **27**, 1 (2019).
- [49] J. Hloušek, M. Dudka, I. Straka, and M. Jeřek, Accurate detection of arbitrary photon statistics, *Phys. Rev. Lett.* **123**, 153604 (2019).
- [50] I. Straka, L. Lachman, J. Hloušek, M. Miková, M. Miřuda, M. Jeřek and R. Filip, Quantum non-Gaussian multiphoton light, *npj Quantum Inf.* **4**, 4 (2018).
- [51] L. Lachman, I. Straka, J. Hloušek, M. Jeřek, and R. Filip, Faithful hierarchy of genuine n-photon quantum non-gaussian light, *Phys. Rev. Lett.* **123**, 043601 (2019).
- [52] L. Lachman and R. Filip, Quantum non-Gaussianity of light and atoms, *Prog. Quantum Electron.* **83**, 100395 (2022).
- [53] D. J. Struik, *Lectures on Classical Differential Geometry* (Addison-Wesley, Reading, MA, 1950).
- [54] R. Horodecki, P. Horodecki, M. Horodecki, and K. Horodecki, Quantum entanglement, *Rev. Mod. Phys.* **81**, 865 (2009).
- [55] N. Brunner, D. Cavalcanti, S. Pironio, V. Scarani, and S. Wehner, Bell nonlocality, *Rev. Mod. Phys.* **86**, 419 (2014).
- [56] A. A. Semenov and A. B. Klimov, Dual form of the phase-space classical simulation problem in quantum optics, *New J. Phys.* **23**, 123046 (2021).
- [57] R. Filip and L. Miřta Jr., Detecting quantum states with a positive wigner function beyond mixtures of gaussian states, *Phys. Rev. Lett.* **106**, 200401 (2011).